DESIGN OF A BRIDGE BUMPER TO PROTECT BRIDGE GIRDERS AGAINST COLLISIONS OF OVERHEIGHT VEHICLES

A Thesis

by

HRISHIKESH SHARMA

Submitted to the Office of Graduate Studies of
Texas A&M University
in partial fulfillment of the requirements for the degree of

MASTER OF SCIENCE

August 2007

Major Subject: Civil Engineering

DESIGN OF A BRIDGE BUMPER TO PROTECT BRIDGE GIRDERS AGAINST COLLISIONS OF OVERHEIGHT VEHICLES

A Thesis

by

HRISHIKESH SHARMA

Submitted to the Office of Graduate Studies of
Texas A&M University
in partial fulfillment of the requirements for the degree of

MASTER OF SCIENCE

Approved by:

Co-Chairs of Committee,	Stefan Hurlebaus
	Paolo Gardoni
Member of Committee,	John Whitcomb
Head of Department,	David Rosowsky

August 2007

Major Subject: Civil Engineering

ABSTRACT

Design of a Bridge Bumper to Protect Bridge Girders against Collisions of Overheight Vehicles. (August 2007)

Hrishikesh Sharma, B.E., Visvesvaraya National Institute of Technology, Nagpur, India

Co-Chairs of Advisory Committee: Dr. Stefan Hurlebaus,
Dr. Paolo Gardoni

Bridges with low clearance are vulnerable to collision with overheight vehicles. Collisions of overheight vehicles can cause fatalities and injuries to the drivers and passengers of the overheight vehicles, and damage to bridge girders. The repair of the damaged bridges can be costly and time consuming. This research investigates the feasibility of developing a bridge bumper that minimizes the physical injuries and the likelihood of fatalities and protects the structural elements of bridges by absorbing the impact energy.

The thesis describes a small-scale impact experiment using the proposed bridge bumper with several options of energy absorbing materials to protect a reinforced concrete beam. A finite element analysis is done to simulate the small-scale impact experiments. Optimization of the finite element model is carried out for the response quantities of interest with respect to the geometrical parameters and the material properties of the proposed bridge bumper. Such analysis can guide the design of an optimal bridge bumper that maximizes the energy dissipation and minimizes the damage to the bridge girder and the likelihood of fatalities and injuries.

ACKNOWLEDGEMENTS

The author takes this opportunity to acknowledge the technical guidance and financial assistance offered by Dr. Stefan Hurlebaus and Dr. Paolo Gardoni during the research period. I thank both of them for entrusting me with this prestigious research work, and helping me at all stages and through all my difficult times. I also thank them for their valuable time and their promptness to clear my doubts anytime I approached them. Without them, this project would not be in its present shape.

I acknowledge all the technical assistance received from Dr. John Whitcomb. I thank him for sharing his technical expertise and helping me improve my model from time to time during the research period.

I acknowledge Texas Transportation Institute (TTI) for partially funding this research project

I also thank my father and mother for their blessings which has made this day possible.

TABLE OF CONTENTS

Page

LIST OF FIGURES

LIST OF TABLES

1. INTRODUCTION

1.1 BACKGROUND

Collisions of overheight vehicles can cause fatalities and injuries to the drivers and passengers of the overheight vehicles, and structural damage to the impacted bridges. This has become one of the most important causes of the damage of bridges in the US and the number of occurrences is likely to increase as new bridges are added to the transportation system (e.g., McCann, 1988; Moss, 1990). The severity of the damages caused by such collisions depends on many factors; like the speed and height of an overheight vehicle and the bridge type.

Several case studies and survey (Feldman et al., 1998; Fu et al., 2001) provide information about fatalities, injuries, and structural damage caused by overheight vehicle collisions and the extent of the problem at state and national level.

Hartik et al. (1990) analyzed 114 bridge failures in the United States over a 38-year period (1951-1988). Out of the 114 failures, 17 (15%) were due to truck collisions. In a similar study, Wardhana and Hadipriono (2003) analyzed 503 bridge failures over an 11-year period (1989-2000) and reported that 14 (3%) bridge failures were caused by collisions of trucks or other vehicles. While overheight vehicle collisions do not always lead to the closure of the impacted bridges, they typically result in damage to bridge girders and vehicles.

This thesis follows the style of *CACAIE Journal.*

A survey conducted by the Texas Department of Transportation (TxDOT) (Feldman et al., 1998) count 241 collisions of overheight vehicles over five years (1987-1992).

Hilton (1973), Hadipriono, (1985) and Humphrey (1988) identify inadequate vertical clearance of bridges as one of the most important factors that might cause collision of vehicles with bridges and point out the need of protection systems for the bridges. To overcome the problem of overheight vehicle collisions, various bridge protection schemes have been investigated and implemented by many Department of Transportations (DOTs).

Protection or prevention schemes can be grouped into four types viz. routing procedures, warning systems, clearance augmentation, and impact absorbers. Prohibiting through-truck movements and routing of overheight vehicles is one of the simplest protective measures (Beckham, 1994). Similarly, Osegueda et al. (1999) developed a Geographical Information System (GIS) based network routing procedure for oversized vehicles, but these systems are cumbersome and often inefficient. Hanchey and Exley (1990) investigated some basic bridge warning schemes, but they have several disadvantages including being costlier (Bowman, 1993) and inadequate for proper warning. In Georgia some bridges have been rehabilitated by the Georgia Department of Transportation (GDOT) using steel pedestals to increase the vertical clearance of bridges. However, steel pedestals may exhibit structural instability under horizontal loads (Hite and DesRoches, 2006). Also, the installation process may require

closure of the bridge, thereby proving to be cumbersome. The fourth category of bridge protection system consists of passive vibration absorbers that are directly attached to the bridge girder. For example, TxDOT implemented vibration absorbers on some prestressed highway bridge girders (Figure 1.1). However, this system does not have the adequate capacity to withstand the severe impact of an overheight vehicle. Qiao et al. (2004) developed an overheight collision protection sandwich system for concrete girders. However, the response of the girders was not evaluated, thus not addressing the fundamental issue of the effectiveness of the protection system.

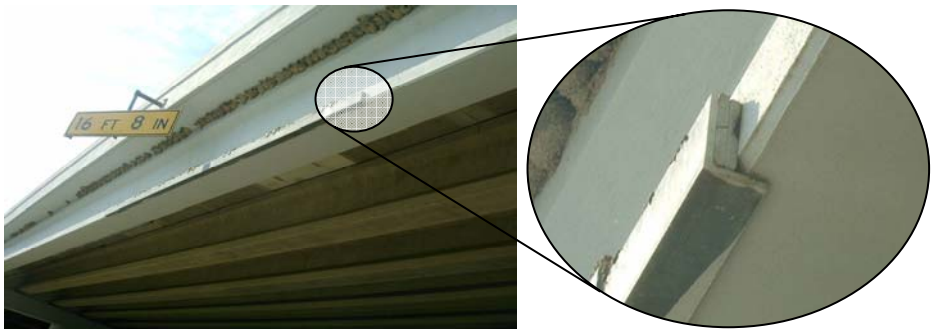

Figure 1.1: Vibration absorber attached to a prestressed bridge girder on Texas State Highway 6

1.2 PROBLEM STATEMENT AND RESEARCH OBJECTIVE

This thesis proposes a protection system, herein called *bridge bumper* that consists of two elements, a *stiff guard* and an *energy absorbing material* (EAM). The stiff guard is used to distribute the concentrated impact of an overheight vehicle over a larger area, thereby decreasing stress concentration at the point of impact. The stiff guard is attached to the bridge girder with an underlying layer of EAM. The EAM is designed to dissipate the impact energy. Figure 1.2 shows the sketch of the proposed bridge bumper. The goal of this work is to show the benefits of proposed bridge bumper.

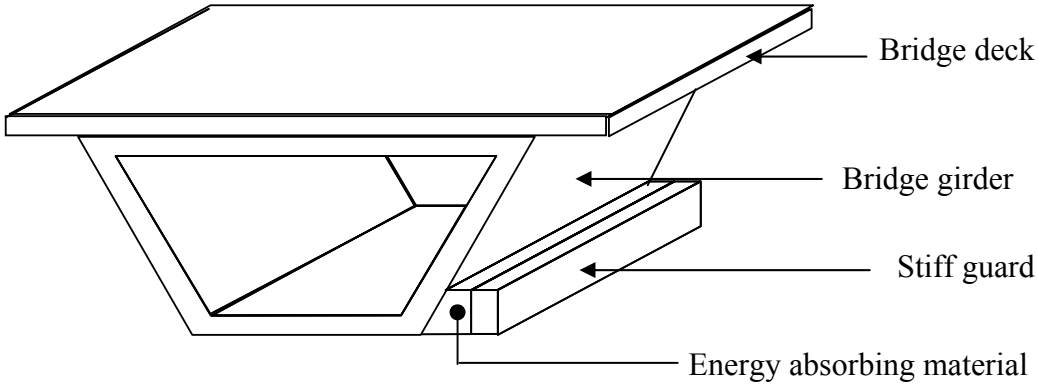

Figure 1.2: Sketch of the proposed bridge bumper for a bridge girder

1.3 THESIS ORGANIZATION

This thesis includes seven sections and several subsections. Following this introduction, I describe the experiments conducted on a small-scale model of the bridge bumper. Then, a finite element model (FEM) of the experimental setup of the reinforced concrete (RC) beam with bridge bumper is presented. Next, I validate the FEM model with the experimental results and investigate the effects of the proposed bridge bumper on the stress reduction and energy absorption. After that I optimize the material and geometric parameters to maximize the benefits of the bridge bumper. Finally, I conclude the thesis by assessing the performance of the bridge bumper as a protection system and present recommendations for the future work.

2. EXPERIMENTAL SETUP AND PROTOCOL

To investigate the potential benefits of the proposed bridge bumper, a small-scale experimental setup of a prototype of the bridge bumper is prepared and impact experiments are conducted. The experimental setup gives the actual behavior of the bridge bumper and determines its effectiveness by evaluating the recorded responses. During the impact testing, measurements of the accelerations of the RC beam are recorded.

The experimental set up is prepared to examine the effect of vehicle impact on a bridge girder. The bridge girder is modeled by simply supported RC beam which is usually taken as the boundary condition for a bridge girder. The weight of the solid steel balls (impactors) is chosen so that the RC beam remains in the elastic range during impact. The impact is done by dropping impactors on the RC beam due to the effect of gravity. This process is chosen because it can be easily incorporated in a FEM. The thickness of the EAM is kept about half of the thickness of the RC beam in order to study the effect of the energy absorption capacity of the EAM. The reduction in responses is tried to achieve by the effect of the total energy absorbed rather than by only increasing the thickness of EAM. The material of stiff guard is chosen to be of steel. Steel has large rigidity; so it can distribute the impact on a large area, thereby engaging large percentage of EAM for reducing the responses.

The experimental set up for the impact testing of the bridge bumper consists of an RC beam, a layer of EAM and a stiff guard. The beam represents a bridge girder. It

is 1.04 m long, with a cross sectional area of 105×103 mm^2. It is reinforced with two number four bars (2 nos. #4) (12.54 mm diameter) at 20 mm from the bottom face. Table 2.1 gives the material properties of the RC beam. The bridge bumper consists of a layer of stiff guard and EAM. In this study four different types of the Last-A-Foam series of foams are used as EAM. The four foams are labeled as A, B, C, and D. Table 2.2 (Sharma et al., 2007) described their material properties. The foams are high density flexible polyurethane foams and are 50 mm thick. They have a flat static and dynamic stress versus deflection curves which makes them suitable for absorbing large amount of impact energy (Sharma et al., 2007).

Table 2.1: Material properties of RC beam and stiff guard

Material	**Density ρ [kg/m3]**	**Modulus of Elasticity E [GPa]**	**Poisson's ratio υ**	**Unconfined Compressive Strength [MPa]**	**Unconfined Tensile Strength [MPa]**	**Yield Stress [MPa]**
Concrete	2500	35.6	0.2	96.0	7.0	-
Steel	7850	167	0.3	-	-	772

Table 2.2: Types of EAM used in the experiment

Label	**Type**	**Density [kg/m^3]**	**Modulus of elasticity [GPa]**	**Hyteresis [%]**
A	EF-4003-06	93.22	5.62E−4	51
B	EF-4004-04	68.20	1.10E−4	51
C	TF-6070-15	240.0	1.82E−3	51
D	TF-5070-13	217.0	6.89E−4	51

EAM A is used for vibration isolation and cushioning for loads in the 689 N/m^2 to 13,789 N/m^2 static stress load range. EAM B is the fire resistant version of EAM A. EAM C is used for shock isolation in instrument floors, missiles and as shipping pads. Its application range for continuous static stress load is from 1,378 N/m^2 to 68,947 N/m^2. EAM D is the fire resistant counterpart of EAM C. The stiff guard is attached to the layer of EAM and is 3.75 mm thick, and the whole assembly is fixed on the RC beam.

Solid steel balls having varying weights are used as impactors. Table 2.3 lists the diameter and weight for each steel ball. In this experiment, the steel balls are released from 1.75 m and attain a calculated velocity of 5.914 m/s at the moment of impact.

Table 2.3: Types of steel balls (impactors) used in the experiment

Label	Diameter [mm]	Weight [g]
1	25.4	67
2	38.1	228
3	50.8	540

An accelerometer (Brüel & Kjær Type 4383) is used to measure the acceleration of the RC beam. The accelerometer is centered on the opposite face of the RC beam with respect to the point of impact, and is connected to a conditioning amplifier (Brüel & Kjær Type 2692-A-0I4). The conditioning amplifier, used for recording of vibration signals, is connected to a digital storage oscilloscope (Tektronix TDS 2014) which is connected to a computer using serial binary data interconnection (RS232). Figure 2.1 depicts the experimental setup.

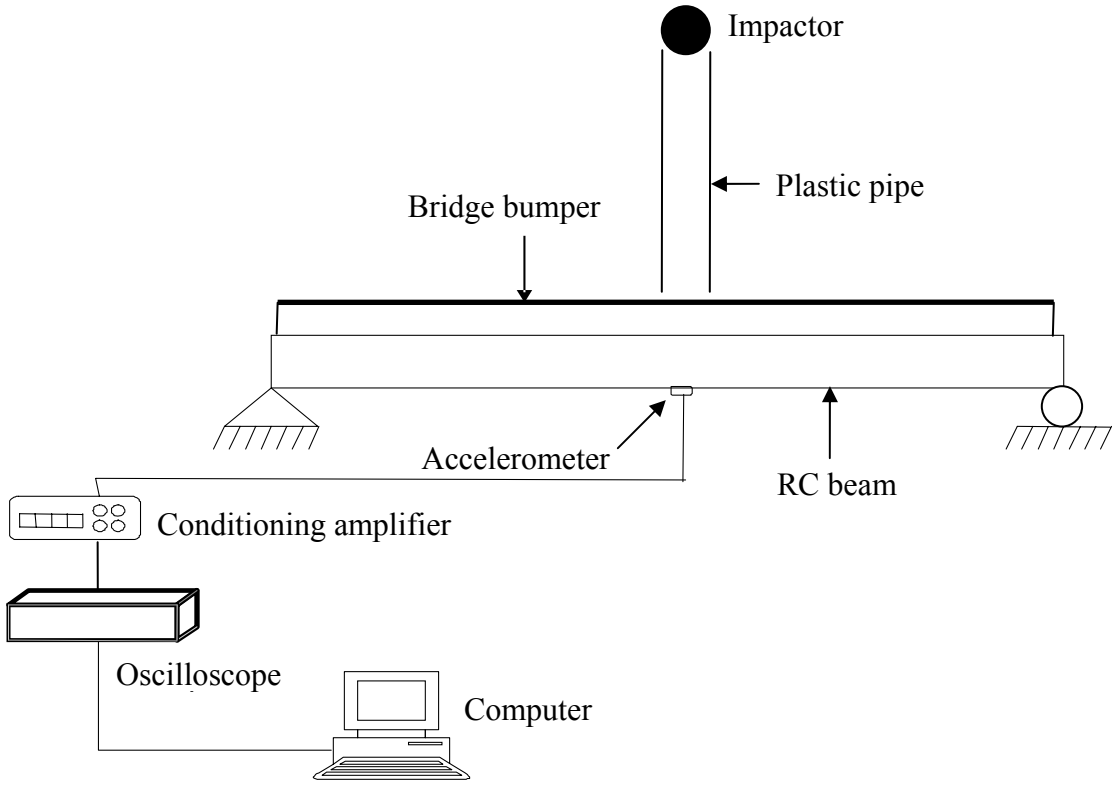

Figure 2.1: Experimental setup for the impact testing on bridge bumper

Three experimental configurations are considered. First, the accelerations are measured for the RC beam without the bridge bumper. Then, measurements are repeated using the RC beam with the stiff guard only. Finally, measurements are taken using the bridge bumper.

3. FINITE ELEMENT MODEL

A FEM of the RC beam and the bridge bumper is developed and validated with the experimental results. The FEM gives the advantage of providing any response of interest and allows changing the values of the parameters, which would have otherwise proven to be expensive or impossible to implement in the experimental setup. The FEM is used to assess and study the effects of the bridge bumper on stresses, contact force and energy absorption.

In this study, the commercial finite element program LS-DYNA is used for the finite element analysis (Livermore Software Technology Corporation, 2003, 2006). The FEM's meshing in this research is generated using HyperMesh (Altair Engineering, 2003a, b).

In this thesis, a smeared model is used for the RC beam. The material type '84-85 Winfrith Concrete' is used for the smeared-crack smeared-rebar model. The RC beam and EAM is modeled by fully integrated quadratic 8 node element with nodal rotations. The material formulation used for the EAM is 'Mat_Low_Density_Foam (MAT_057)' available in LS-DYNA. This model can characterize the high compressibility and rate sensitivity of the low density urethane foam materials used in the experimental tests. The compressive behavior under uniaxial loading is assumed to remain uncoupled in the transverse direction. In tension a linear behavior is exhibited until tearing. The rate effects are accounted by using linear visco-elastic model. The stiff guard is modeled using an elasto-plastic material formulation. The impactors are

modeled as rigid body using the material properties of steel. The penalty method is used to model the contacts between the different elements. In this method normal interface springs are placed between all penetrating nodes and the contact surfaces. This method is stable and it does not excite mesh hourglassing. It is capable of handling contacts between dissimilar metals like steel-foam or concrete-foam which is well suited for this study.

4. VALIDATION

The acceleration-time-histories of the FEM models are compared with the experimental results. Figures 4.1-4.5 shows the recorded and simulated accelerations for Impactor 1. The accelerations are shown for the RC beam without the bridge bumper (Figure 4.1), the RC beam with the stiff guard only (Figure 4.3), and the RC beam with the bridge bumper (Figure 4.5). The acceleration profiles of FEM simulation are shown by dashed lines and the experimental results are shown by solid lines. The time period as well as the amplitude of the acceleration profiles are of the same order and compares well for all of the configurations. The scale for the magnitude is kept constant in all the Figures 4.1-4.5 for the comparison reasons.

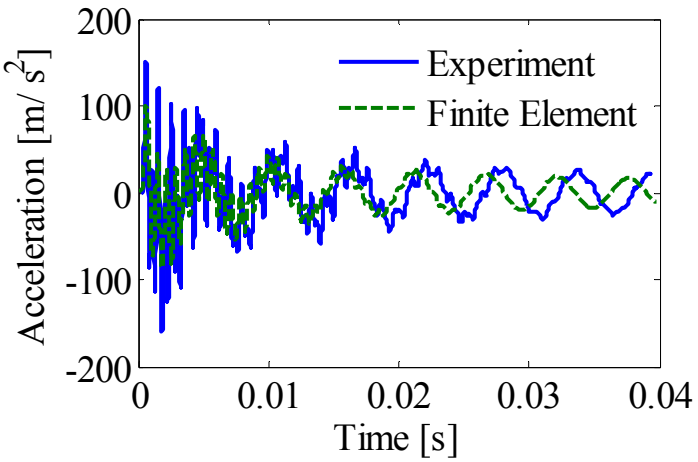

Figure 4.1: Acceleration-time-history of experiment and finite element simulation for the beam without protection system (Impactor 1)

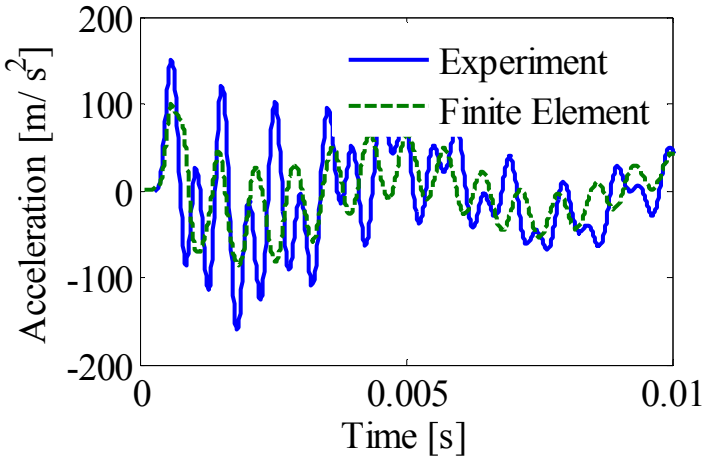

Figure 4.2: Enlarged view of acceleration-time-history of experiment and finite element simulation for the beam without protection system (Impactor 1)

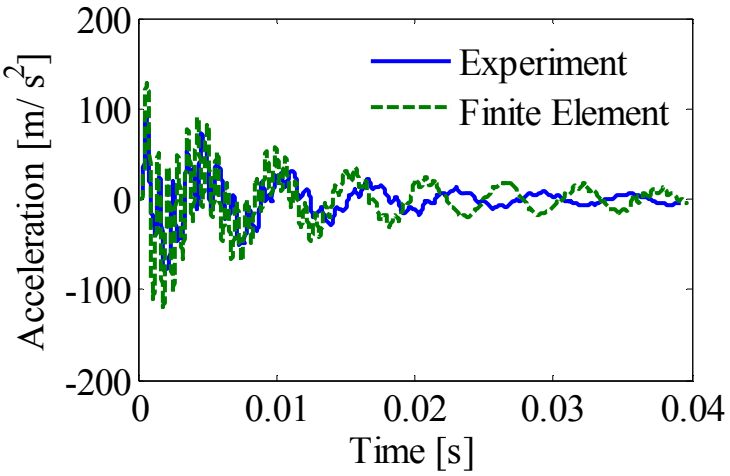

Figure 4.3: Acceleration-time-history of experiment and finite element simulation for the beam with stiff guard (Impactor 1)

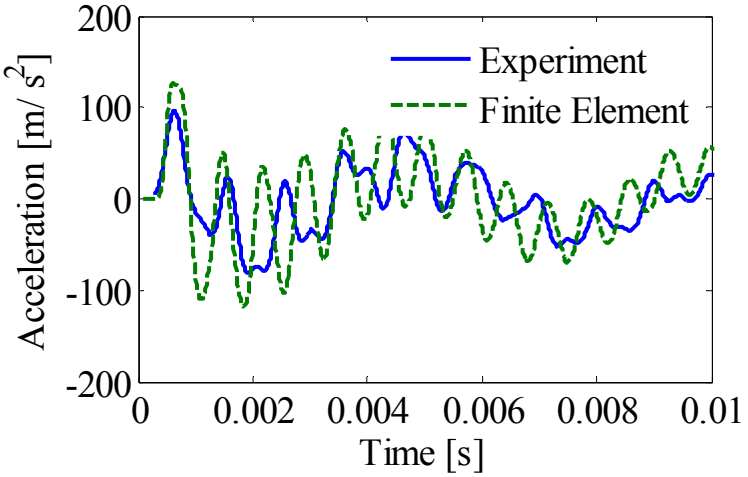

Figure 4.4: Enlarged view of acceleration-time-history of experiment and finite element simulation for the beam with stiff guard (Impactor 1)

The magnitude of acceleration during impact compares well for the case of unprotected beam and beam with stiff guard as seen in the enlarged view of Figure 4.2 and Figure 4.4. The high frequency vibration is due to the noise recorded by the instrument. The source of the noise can be attributed to the vibration caused by the supporting frame of the experimental setup, the excitation of the higher modes and the inherent noise of the instruments. The high frequency waves are reduced in case of RC beam with bridge bumper as shown in Figure 4.5. This may be due to the fact that the EAM damp out the vibration and the higher modes are not excited. Also the overall vibration in the supporting frame is reduced. The magnitude of acceleration during impact is less than the second cycle in case of RC beam with bridge bumper (Figure 4.5). This is possibly due the following reason. When the impactor hits the system, the impact first propagates through the EAM and due to its absorbing capacity the RC beam

is not fully excited, hence the acceleration remains low in the first cycle. The RC beam is then fully excited in the second cycle when the impact fully propagates through the RC beam, hence the acceleration is higher in the next cycle. Figure 4.5 shows a damped acceleration profile as compared to Figures 4.1 and 4.3 which is due to the effect of EAM. Overall, the time period and amplitudes are modeled within comparable range thus establishing the fact that the dynamics of the system is accurately modeled. The accelerations for Impactors 2 and 3 are not shown here for sake of brevity. However, similar observations can be made.

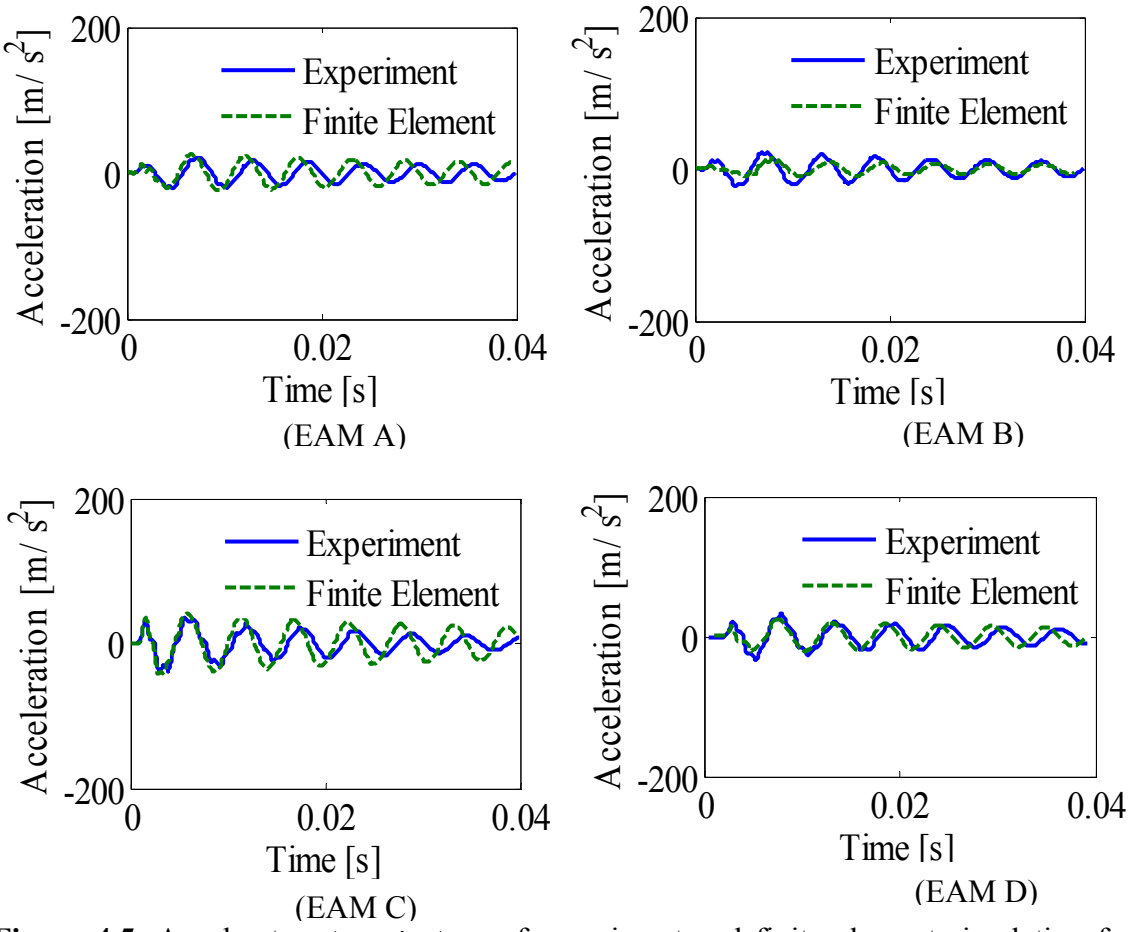

Figure 4.5: Acceleration-time-history of experiment and finite element simulation for the RC beam with different EAM used for bridge bumper

5. DISCUSSION

In order to demonstrate the efficiency of the proposed bridge bumper, Table 5.1 compares various response parameters for each configuration and selection of EAM. The maximum compressive and tensile stresses occurring in the RC beam are important criterion for its performance. The maximum stresses were calculated at the centre of the RC beam at the point of impact by the impactors and at point directly opposite to the point of impact on the other face of RC beam. The table reports the tensile and compressive stresses in the RC beam, the energy absorbed by the EAM, the contact force, and the absolute values of maximum and minimum acceleration-time-histories. Percent reductions are computed using the results for the bare RC beam as baseline. The following observations can be made: the proposed bridge bumpers reduce stresses by 98% while only 50% is achieved for the stiff guard alone. The internal absorbed energy is more for EAM D and C than EAM A and B. The bridge bumpers achieve a reduction up to 96% for the contact force. The stiff guard results in an increase of 79% for the contact force. The introduction of stiff guard results in an increase in the overall stiffness. This increased stiffness results in a proportional increase in the contact force. The bridge bumper reduces the values of the peak acceleration by 72%-86%. EAM B provides the largest reduction. Whereas, the stiff guard alone provides a reduction of 26%. The performance of EAM A, EAM B and EAM D are similar to each another. The performance of EAM C varies from the rest owing to its larger stiffness. The reduction of stresses, contact force and acceleration is more for EAM A and EAM B than EAM C

and EAM D. The results in Table 5.1 clearly demonstrate the effectiveness of bridge bumper as a protection system for the RC beam.

Table 5.1: Comparison of simulated responses for different configurations using Impactor 1

Configuration	Tensile stress [MPa]	Compressive stress [MPa]	Energy absorbed by EAM [Nm]	Contact force of beam [kN]	Abs. max. acceleration [m/s^2]	Abs. min. acceleration [m/s^2]
Beam without bridge bumper	1.76	17.0	0.00	7.77	151.3	160.9
Beam with stiff guard	1.64 (−7%)	8.57 (−50%)	0.00	13.9 (79%)	127.5 (−16%)	118.0 (−26%)
Bridge bumper with EAM A	0.58 (−67%)	0.66 (−96%)	0.32	0.49 (−94%)	26.4 (−82%)	24.5 (−85%)
Bridge bumper with EAM B	0.47 (−73%)	0.43 (−98%)	0.24	0.31 (−96%)	21.5 (−85%)	22.5 (−86%)
Bridge bumper with EAM C	1.41 (−20%)	1.36 (−92%)	0.50	0.92 (−88%)	41.7 (−72%)	42.6 (−74%)
Bridge bumper with EAM D	0.65 (−63%)	0.56 (−97%)	0.42	0.47 (−94%)	32.1 (−78%)	37.8 (−77%)

These results demonstrate that the proposed bridge bumper significantly reduces the acceleration of the bridge girder as well as the impact force. Furthermore, the result shows that longitudinal stresses in the bridge girder are reduced using the bridge bumper. The EAM B used in the study proves to be the most efficient amongst all the EAM as maximum reduction in all the response quantities is obtained by it. So, overall, all calculated responses that are crucial to the RC beam's performance are reduced. While the performance level of the different energy absorbing materials varies, the overall efficiency of a bridge bumper is demonstrated.

6. OPTIMIZATION

The efficient design of a system relies on the optimal selection of material properties and geometry to maximize the desired performance. To achieve this goal, the optimization of the bridge bumper is done to achieve a better protection of the RC beam. In this section, the material and geometric properties of the bridge bumper are optimized by minimizing the sum of the maximum tensile and compressive stresses in the beam. Tensile and compressive stresses are selected because they are the potential causes for the failure of a RC beam during an impact. Next, the stress profiles, the energy absorbed by EAM, the contact forces, and the acceleration-time-histories of the RC beam with bridge bumper are compared with those obtained without the bridge bumper to determine the effectiveness of the optimization.

The optimization of the geometry and material properties is done by using the optimization software LS-OPT. The three parameter classical Kelvin-Voigt viscoelastic material formulation is used to model the EAM for the parametric evaluation of the properties. The six different design variables used for the optimization of EAM are the density ρ, the elastic bulk modulus B, the short term shear modulus $G(0)$, the ratio between long term shear modulus $G(\infty)$ and short term shear modulus $G(0)$ defined as $r_G = G(\infty)/G(0)$, the decay constant τ_{R}, and the ratio r_{EA} between thickness of the EAM and the total thickness of bridge bumper. The total thickness t_{Total} of the bridge bumper is held constant so the expression $t_{\mathrm{Total}}(1-r_{\mathrm{EA}})$ gives the optimized thickness of the stiff guard. The response surface methodology (RSM) with quadratic approximation

order is chosen for the optimization process (Myers and Montgomery, 1995). The methodology requires the analysis of a predetermined set of designs. A design surface is then fitted to the response values using regression analysis. Finally, the response surface is used to construct an approximate design sub-problem which is then optimized. The method has the tendency of capturing globally optimal regions and thus local minima can be avoided. The D-optimal scheme (Myers and Montgomery, 1995) is used for the point selection. This scheme is used for the selection of best set of points for the response surface from a given set of points.

The results of the optimization on the response function stress are described below. The value of the coefficient of multiple determination R^2 for the quadratic approximation is 0.858 for both the tensile and compressive stresses. The expression for R^2 is

$$R^2 = \frac{\sum_{i=1}^{P} \left(\hat{y}_i - \overline{y}_i \right)^2}{\sum_{i=1}^{P} \left(y_i - \overline{y}_i \right)^2} \tag{6.1}$$

where, P = the number of design points

$\overline{y}_i$ = the mean of the responses,

$\hat{y}_i$ = the predicted response, and

y_i = the actual response.

The root mean square (RMS) error for the response function for the tensile stress is 9.37% and for the compressive stress is 10.35%. These values indicate that a good agreement is obtained between the predicted and computed stress values, thus justifying

the use of quadratic approximation. The convergence of the stresses is reached in three iterations with the values converging to 0.35 MPa for both compressive and tensile stresses. Table 6.1 lists the optimized value of the parameters. These parameters represent values that can be used in practice to design a bridge bumper for the RC beam used in the present study. Table 6.2 gives the responses of the quantities of interest for this optimization process. The values are compared with the unprotected RC beam. There is a significant reduction for all the quantities of interest. The maximum stresses reduce by 80-98 % whereas the contact force reduces by 58 %. The accelerations also decrease by 53 %.

Table 6.1: Optimized value of the variables

Variables	Value
ρ [kg/m^3]	915.3
B [GPa]	9.60
$G(0)$ [GPa]	4.85
$r_G = G(\infty)/G(0)$	0.401
$G(\infty)$ [GPa]	1.95
τ_R [s]	0.0095
r_{EA}	0.375

Table 6.2: Comparison of responses due to Impactor 1 for the optimized material and geometrical properties vs. the beam without bridge bumper

Configuration	Beam without bridge bumper	Optimized bridge bumper
Tensile stress [MPa]	1.76	0.35 (−80%)
Compressive stress [MPa]	17.0	0.35 (−98%)
Energy absorbed by the EAM [Nm]	0.00	0.03 (N/A)
Contact force RC beam [kN]	7.77	3.3 (−58%)
Absolute max. acceleration [m/s^2]	150.3	70.0 (−53%)
Absolute min. acceleration [m/s^2]	160.9	80.0 (−50%)

It is crucial in the design process to study the dependency of response quantities i.e., tensile and compressive stresses on the material and geometric properties. The contour plots for the response quantities are plotted by varying different parameters used in the optimization (Figure 6.1-6.2). The optimized value for the different parameters is shown by a dot (●) in the contour plots. The tensile stress decreases with an increase in the density ρ of EAM from 300 kg/m^3 up to value of approximately 1950 kg/m^3 and then increases with a further increase in the value of density ρ. The tensile stress increases with an increase in value of bulk modulus B of EAM up to approximately 12 GPa and then again decrease with an further increase in value of bulk modulus (Figure 6.1 (a)). The tensile stress decreases with an increase in short term shear modulus $G(0)$ of EAM. The increase in modulus ratio r_G also results in a decrease of tensile stress (Figure 6.1 (b)). The tensile stress increases with increase in the decay constant τ_R of EAM. The thickness ratio r_{EA} of EAM achieves an optimum around 0.4 with value of stress decreasing below this value and increasing above it (Figure 6.1 (c)).

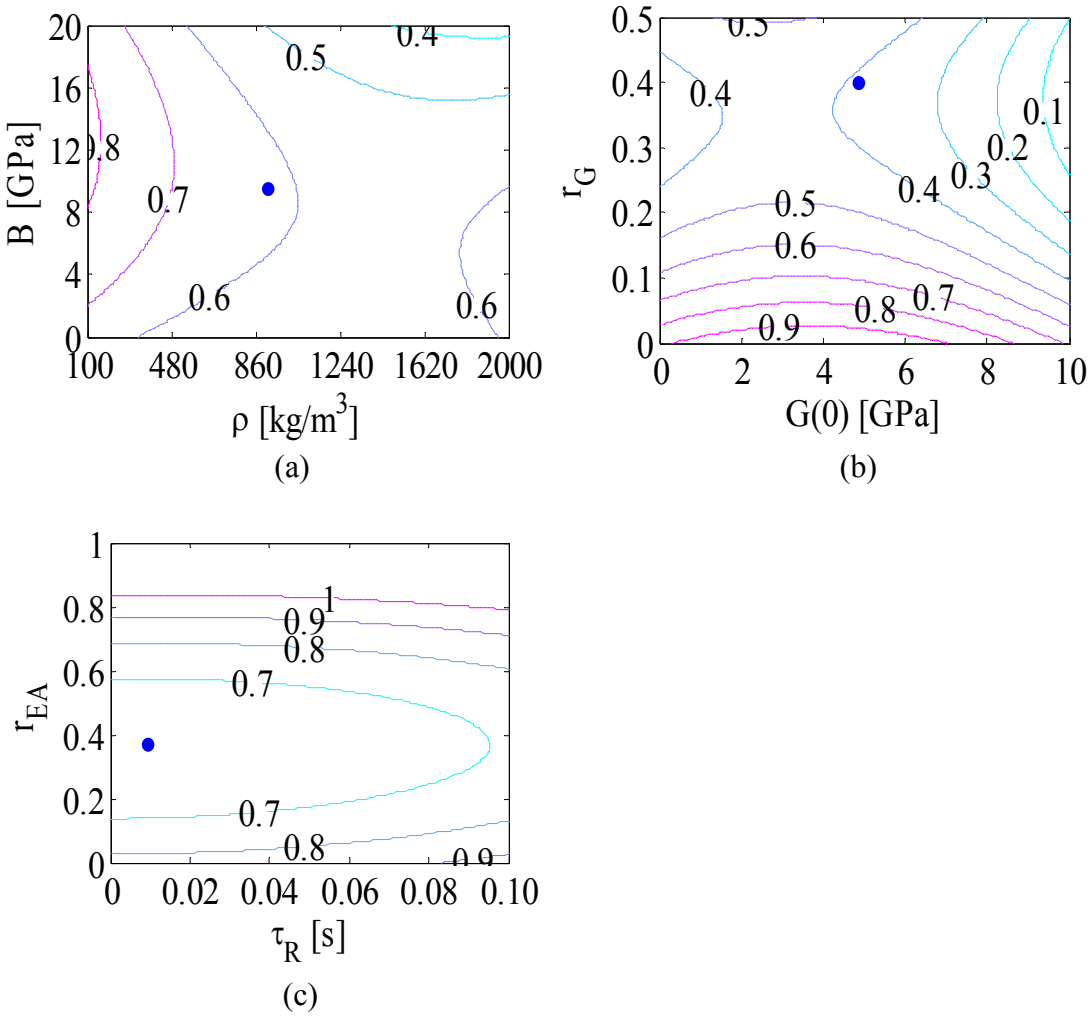

Figure 6.1: Contour plots of tensile stress with variation of (a) density and bulk modulus (b) shear modulus of EAM (c) decay constant and ratio of thickness of EAM

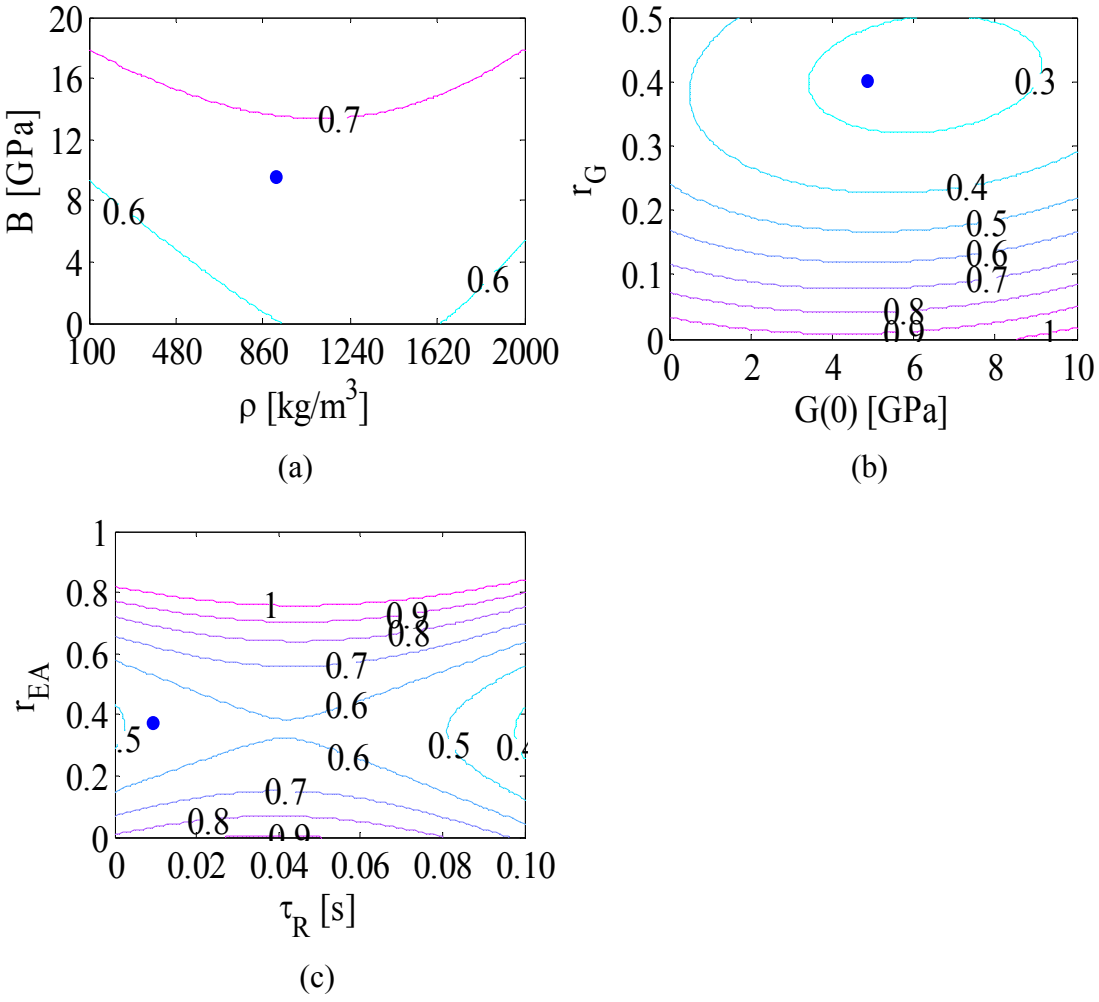

Figure 6.2: Contour plots of compressive stress with variation of (a) density and bulk modulus (b) shear modulus of EAM (c) decay constant and ratio of thickness of EAM

Figure 6.2 shows the variation of compressive stress with various parameters used in optimization. The compressive stress decreases with an increase in density ρ of EAM up to 860 kg/m^3 and then increases with a further increase in the value from 1620 kg/m^3. The comparison of both the response shows that an ideal case will be to have a material in the 300 kg/m^3 to 900 kg/m^3 range while a range of 1600 kg/m^3 to 1950

kg/m^{3}can also reduce the stresses. The compressive stress increases with an increase in the value of bulk modulus B (Figure 6.2 (a)). The compressive stress remains approximately constant by a variation in short term shear modulus $G(0)$ of EAM while it decreases with an increase in modulus ratio r_G (Figure 6.2 (b)). The increase in the decay constant τ_R of EAM results in slight decrease in compressive stress. The compressive stress follows the same trend as the tensile stress for the variation of the thickness ratio r_{EA} of EAM with an optimum around 0.4 (Figure 6.2 (c)). The optimized values of both the responses in Figures 6.1-6.2 do not fall in the absolute minimum region for any of the two stresses. This is due to the fact that the optimization function is the sum of the maximum tensile and compressive stresses and not their individual values. Thus the optimal value is a compromise between the two stresses.

This parametric study gives a useful guideline for effectively choosing the geometric and material property for the design of the bridge bumper. The material property of the EAM should be chosen so that the candidate material has a) density ρ in the range from approximately 300 kg/m^3 to 900 kg/m^3 and in range of 1600 kg/m^3 to 1950 kg/m^3 b) less bulk modulus B, c) large short term shear modulus $G(0)$, and d) small value of decay constant τ_R. The modulus ratio r_G should be maximized up 0.4-0.5 to achieve maximum stress reduction. The ratio of the thickness of the EAM r_{EA} should be maximized up to 40% of the total thickness of the bridge bumper (within the design constraint of the total thickness of bridge bumper) to achieve a maximum stress reduction in the system.

7. CONCLUSIONS

The present work establishes the effectiveness of a bridge bumper system as a protection system for bridge girders. It proves that the responses of concern for a bridge system subject to a vehicle impact can be significantly reduced by introducing a protection system. An optimization of the material and geometric property of the energy absorbing material and stiff guard was carried out and optimal values that can be used in practice were obtained. A guideline for effectively choosing the material property and geometry was also established.

A detailed study is underway to test a full-scale bridge bumper. The results of this research can be used to design a bridge bumper that can effectively mitigate the problem of overheight collision, thereby reducing the number of fatalities and repairing cost of the bridge girders. This type of protection system can find wide application such as designing protection system against blast loads, impact protection systems in piers, etc.

REFERENCES

Altair Computing (2003a). *HyperMesh Ver. 6.0 Basic Tutorial*, Altair Engineering Inc., Troy, MI.

Altair Computing (2003b). *HyperMesh Ver. 6.0 Advanced Tutorial*, Altair Engineering Inc., Troy, MI

Beckham, S. (1994). *"Regional Trucking Issues: Truck Route Alternatives, Geometric Consideration for Large Trucks, and Regulation of Texas Trucking."* Report for North Central Texas Council of Governments, Arlington, TX.

Bowman, B. L. (1993). *Supplemental Advance Warning Devices*. National Cooperative Highway Research Program, Synthesis of Highway Practice Report 186. Transportation Research Board, National Research Council, National Academy Press, Washington, DC.

Feldman, L. R., Jirsa, J. O., and Kowal, E. S. (1998). Repair of bridge impact damage. *Concrete International*, **20**(2), 61-66.

Fu, C. C., Burhouse, J. R., and Chang G. (2001). Study of overheight vehicle collisions with highway bridges. *Transportation Research Records*, **1865**, 80-88.

Hadipriono, F. C. (1985). Analysis of events in recent structural failures. *Journal of Structural Engineering*, **111**(7), 1468-1481.

Hanchey, C. M., and Exley, S. F. (1990). Overheight vehicle warning systems in mississippi. *ITE Journal*, **60**(6), 24-29.

Hartik, I. E., Shaaban, A. M., Gesund, H., Valli, G. Y. S., and Wang S. T. (1990). United States bridge failures, 1951-1988. *Journal of Performance of Construction Facilities*, **4**(4), 272-277.

Hilton, M. H. (1973). Some case studies of highway bridges involved in accidents. *Highway Research Board*, **432**, 41-51.

Hite, M., and DesRoches, R. (2006). Seismic performance of bridge steel pedestals, *Proceedings of the 5th National Seismic Bridge Conference*, San Francisco , CA, September, 2006.

Humphrey, T. F. (1988). *Uniformity Efforts in Oversize/Overweight Permits*. National Cooperative Highway Research Program Report 143, Transportation Research Board, Washington, DC.

Livermore Software Technology Corporation (2003). *LS-DYNA Keyword User's Manual*. Version 970, Livermore, CA.

Livermore Software Technology Corporation (2006). *LS-OPT User's Manual*. Version 3.1, Livermore, CA.

McCann, V. (1988). An overheight-vehicle detection system. *Traffic Engineering and Control*. **29**(4), 210-215.

Moss, C. (1990). Failsafe, remotely monitored overheight vehicle measurement system. *Australian Road Research Board Proceedings*, part **6**, 15th ARRB Conference, 115-126.

Myers, R.H., Montgomery, D.C. (1995) *Response Surface Methodology. Process and Product Optimization using Designed Experiments.* Wiley, Hoboken, NJ.

Osegueda, R., Garcia-Diaz, A., Ashur, S., Melchor, O., Chang, S., Carrasco, C., and Kuyumcu, A. (1999). GIS-based network routing procedures for overweight and oversized Vehicles. *Journal of Transportation Engineering*, **125**(4), 324-331.

Qiao, P., Yang, M., and Mosallam, A. S. (2004). Impact analysis of I-Lam sandwich system for over-height collision protection of highway bridges. *Engineering Structures*, **26**, 1003-1012.

Sharma, H., Hurlebaus, S., Gardoni, P. (2007), Bridge bumper concept and FEA-based design methods to protect bridge girders from overheight vehicle impacts. Submitted to *Computer-Aided Civil and Infrastructure Engineering.*

Wardhana, K., and Hadipriono, F. C. (2003). Analysis of recent bridge failures in the United States. *Journal of Performance of Construction Facilities*, **17**(3), 144-150.

APPENDIX A

The acceleration-time-histories of the FEM models are compared with the experimental results. Figures A.1-A.3 shows the recorded and simulated accelerations for Impactor 2. The accelerations are shown for the RC beam without the bridge bumper (Figure A.1), the RC beam with the stiff guard only (Figure A.2), and the RC beam with the bridge bumper (Figure A.3). The acceleration profiles of FEM simulation are shown by dashed lines and the experimental results are shown by solid lines. The time period as well as the amplitude of the acceleration profiles are of the same order and compares well for all of the configurations. The scale for the magnitude is kept constant in Figures A.1-A.3 for the comparison reasons. The response of bridge bumper using EAM B does not compare well. This may be attributed to the fact that exact stress-strain curve for the given specimen is not available. Only the representative curve for EAM B is used which compares well for low strains, but exhibit differences with increased strains. Overall, the time period and amplitudes are modeled within comparable range thus establishing the fact that the dynamics of the system is accurately modeled.

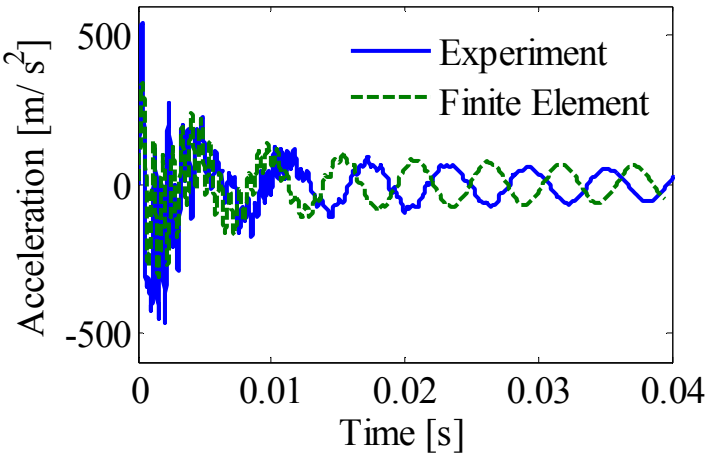

Figure A.1. Acceleration-time-history of experiment and finite element simulation for the beam without protection system (Impactor 2).

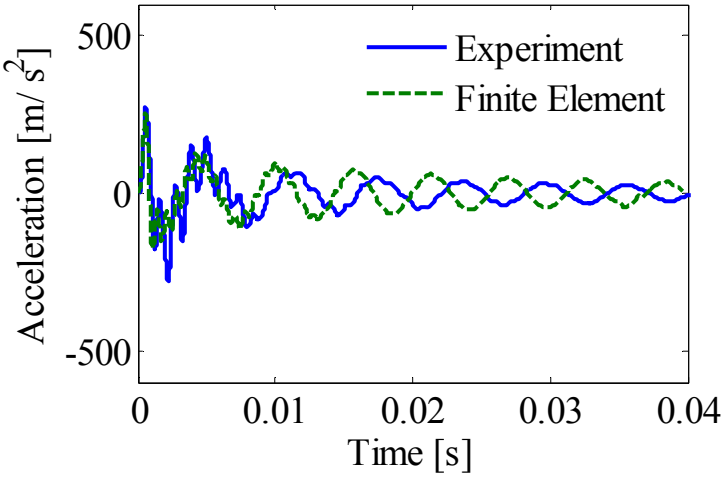

Figure A.2. Acceleration-time-history of experiment and finite element simulation for the beam with stiff guard (Impactor 2).

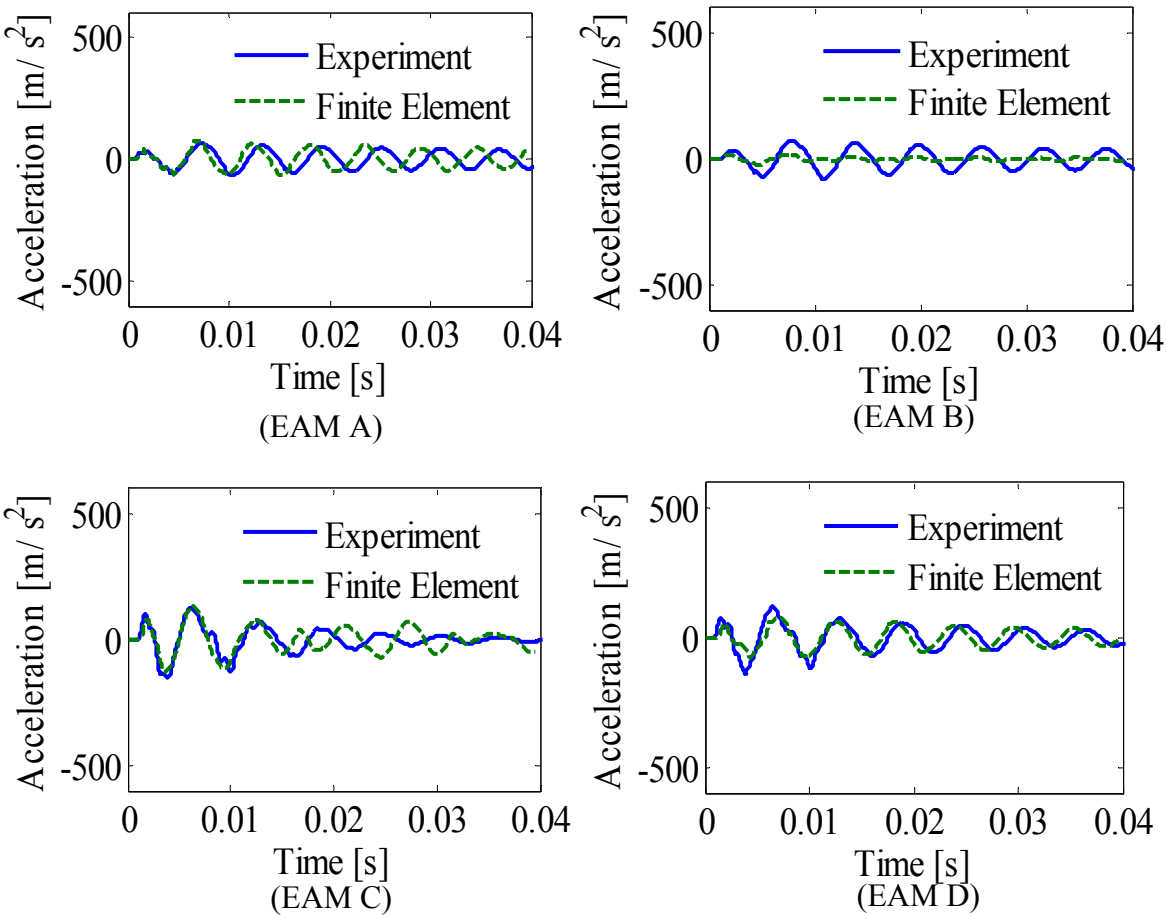

Figure A.3. Acceleration-time-history of experiment and finite element simulation for the RC beam with different EAM used for bridge bumper (Impactor 2).

APPENDIX B

In order to demonstrate the efficiency of the proposed bridge bumper, Table B.1 compares various response parameters for Impactor 2 for each configuration and selection of EAM. The maximum compressive and tensile stresses occurring in the RC beam are important criterion for its performance. The maximum stresses were calculated at the centre of the RC beam at the point of impact by the impactors and at point directly opposite to the point of impact on the other face of RC beam. The table reports the tensile and compressive stresses in the RC beam, the energy absorbed by the EAM, the contact force, and the absolute values of maximum and minimum acceleration-time-histories. Percent reductions are computed using the results for the bare RC beam as baseline. The following observations can be made: the proposed bridge bumpers reduce stresses up to 93% while only 2% is achieved for the stiff guard alone. The internal absorbed energy is more for EAM C than EAM A and EAM D. The bridge bumpers achieve a reduction up to 96% for the contact force. The stiff guard results in an increase of 159% for the contact force. The bridge bumper reduces the values of the peak acceleration up to 86%. Whereas, the stiff guard alone provides a reduction of 35-50%. The performance of EAM A and EAM D are similar to each another. The performance of EAM C varies from the rest owing to its larger stiffness. The results of EAM B are not considered because the FEM model does not validate well for the comparison of acceleration profile (Figure A.3). The results in Table B.1 clearly demonstrate the effectiveness of bridge bumper as a protection system for the RC beam.

Table B.1. Comparison of simulated responses for different configurations using Impactor 2.

Configuration	Tensile stress [MPa]	Compressive stress [MPa]	Energy absorbed by EAM [Nm]	Contact force of beam [kN]	Abs. max. acceleration [m/s^2]	Abs. min. acceleration [m/s^2]
Beam without bridge bumper	4.42	30.0	0.00	15.0	543.0	428.0
Beam with stiff guard	4.5 (1.8%)	29.4 (−2%)	0.00	38.9 (159%)	272.0 (−50%)	278.0 (−35%)
Bridge bumper with EAM A	2.0 (−55%)	2.0 (−93%)	1.37	1.20 (−92%)	77.0 (−86%)	65.0 (−85%)
Bridge bumper with EAM B	1.2 (−73%)	1.2 (−96%)	1.15	0.74 (−95%)	31.0 (−94%)	69.0 (−84%)
Bridge bumper with EAM C	3.0 (−32%)	3.0 (−90%)	1.60	2.23 (−85%)	104.0 (−81%)	131.0 (−69%)
Bridge bumper with EAM D	2.0 (−55%)	2.0 (−93%)	1.30	1.40 (−91%)	75.0 (−86%)	135.0 (−82%)

The above results are similar to those of the Impactor 1. These results demonstrate that the proposed bridge bumper significantly reduces the acceleration of the bridge girder as well as the impact force. Furthermore, the result shows that longitudinal stresses in the bridge girder are reduced using the bridge bumper. The EAM A and EAM D used in the study prove to be the equally efficient amongst all the EAM as maximum reduction in all the response quantities is obtained by it. So, overall, all calculated responses that are crucial to the RC beam's performance are reduced. While the performance level of the different energy absorbing materials varies, the overall efficiency of a bridge bumper is demonstrated.

APPENDIX C

The acceleration-time-histories of the FEM models are compared with the experimental results. Figures C.1-C.3 shows the recorded and simulated accelerations for Impactor 3. The accelerations are shown for the RC beam without the bridge bumper (Figure C.1), the RC beam with the stiff guard only (Figure C.2), and the RC beam with the bridge bumper (Figure C.3). The acceleration profiles of FEM simulation are shown by dashed lines and the experimental results are shown by solid lines. Experiment was not performed for the RC beam without the bridge bumper. It was done to keep the response in the elastic range so Figure C.1 only shows acceleration response for FEM. The time period as well as the amplitude of the acceleration profiles are of the same order and compares well for all of the configurations. The scale for the magnitude is kept constant in Figures C.1-C.3 for the comparison reasons. The maximum amplitude reached during impact compares well for all the configurations. The mismatch in time period in later phase may be due to the difference in actual stiffness and modeled stiffness of the EAM which is taken as the tangent modulus. Overall, the time period and amplitudes are modeled within comparable range thus establishing the fact that the dynamics of the system is accurately modeled.

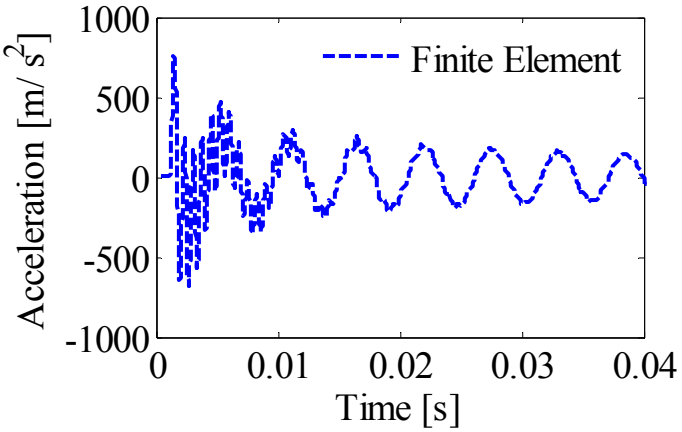

Figure C.1. Acceleration-time-history of experiment and finite element simulation for the beam without protection system (Impactor 3).

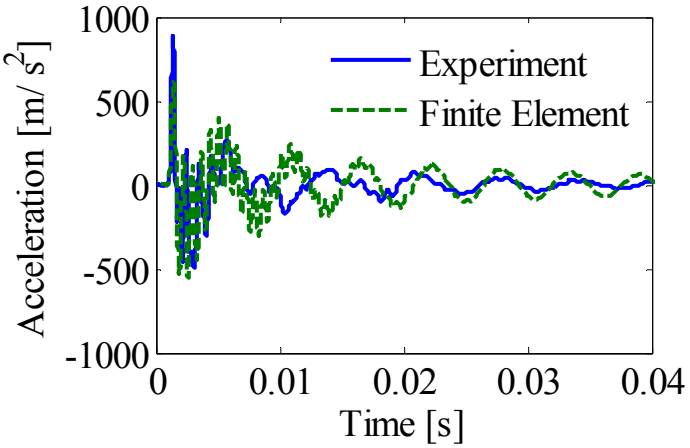

Figure C.2. Acceleration-time-history of experiment and finite element simulation for the beam with stiff guard (Impactor 3).

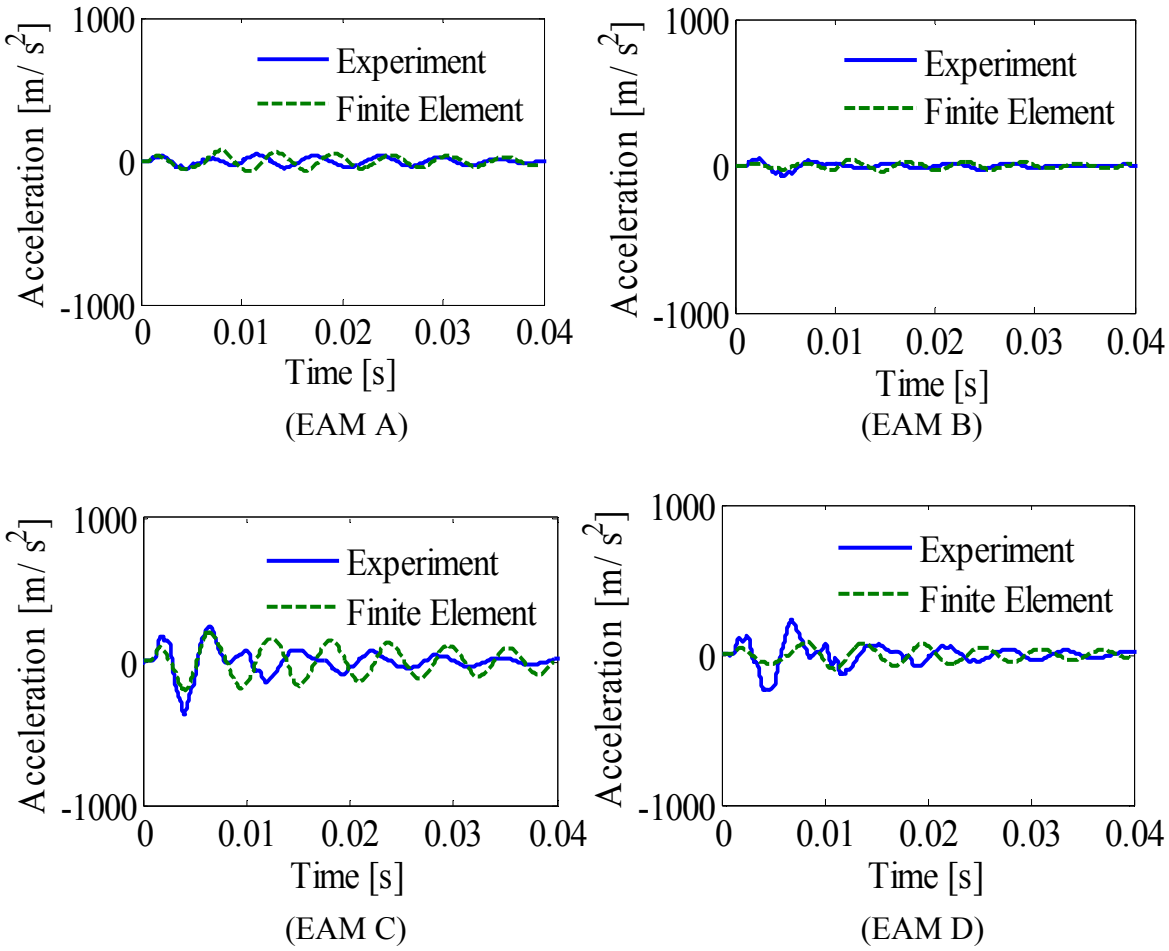

Figure C.3. Acceleration-time-history of experiment and finite element simulation for the RC beam with different EAM used for bridge bumper (Impactor 3).

APPENDIX D

In order to demonstrate the efficiency of the proposed bridge bumper, Table D.1 compares various response parameters for Impactor 3 for each configuration and selection of EAM. The maximum compressive and tensile stresses occurring in the RC beam are important criterion for its performance. The maximum stresses were calculated at the centre of the RC beam at the point of impact by the impactors and at point directly opposite to the point of impact on the other face of RC beam. The table reports the tensile and compressive stresses in the RC beam, the energy absorbed by the EAM, the contact force, and the absolute values of maximum and minimum acceleration-time-histories. Percent reductions are computed using the results for the bare RC beam as baseline. The following observations can be made: the proposed bridge bumpers reduce stresses up to 93% while only 7-13% is achieved for the stiff guard alone. The internal absorbed energy is more for EAM C than EAM A, EAM B and EAM D. The bridge bumpers achieve a reduction up to 95% for the contact force. The stiff guard results in an increase of 40% for the contact force. The bridge bumper reduces the values of the peak acceleration up to 94%. Whereas, the stiff guard alone provides a reduction of 19%. The performance of EAM A and EAM D are similar to each another. The performance of EAM C varies from the rest owing to its larger stiffness. The results in Table D.1 clearly demonstrate the effectiveness of bridge bumper as a protection system for the RC beam.

Table D.1. Comparison of simulated responses for different configurations using Impactor 3.

Configuration	Tensile stress [MPa]	Compressive stress [MPa]	Energy absorbed by EAM [Nm]	Contact force of beam [kN]	Abs. max. acceleration [m/s^2]	Abs. min. acceleration [m/s^2]
Beam without bridge bumper	8.52	38.2	0.00	28.2.0	756.8	682.0
Beam with stiff guard	7.38 (-13%)	35.7 (−7%)	0.00	38.9 (40%)	615.0 (−19%)	552.0 (−19%)
Bridge bumper with EAM A	2.8 (−68%)	2.7 (−93%)	4.42	1.91 (−93%)	42.0 (−94%)	55.0 (−91%)
Bridge bumper with EAM B	1.5 (−82%)	1.5 (−96%)	4.35	1.38 (−95%)	50.0 (−93%)	70.0 (−89%)
Bridge bumper with EAM C	4.6 (−46%)	4.6 (−88%)	5.33	3.18 (−89%)	183.0 (−75%)	364.0 (−47%)
Bridge bumper with EAM D	2.8 (−67%)	2.9 (−92%)	5.15	1.95 (−93%)	128.0 (−83%)	237.0 (−65%)

The above results are similar to those of the Impactor 1 and 2. These results demonstrate that the proposed bridge bumper significantly reduces the acceleration of the bridge girder as well as the impact force. Furthermore, the result shows that longitudinal stresses in the bridge girder are reduced using the bridge bumper. The EAM A and EAM D used in the study prove to be the equally efficient amongst all the EAM as maximum reduction in all the response quantities is obtained by it, which conforms to the result of previous impactors. So, overall, all calculated responses that are crucial to the RC beam's performance are reduced. While the performance level of the different energy absorbing materials varies, the overall efficiency of a bridge bumper is demonstrated.

VITA

Name Hrishikesh Sharma

Address Zachry Department of Civil Engineering

Texas A&M University

College Station

Texas 77840

Email: shrishi@neo.tamu.edu

Education B.E. (Structural) 2003 Visvesvaraya National Institute of Technology, Nagpur, India

MS (Civil Engineering) 2007 Zachry Department of Civil Engineering, Texas A&M University, College Station, TX